



## Effect of long-period ocean tides on the Earth's polar motion

RICHARD S. GROSS<sup>1</sup>, BEN F. CHAO<sup>2</sup> and SHAILEN D. DESAI<sup>1</sup>

<sup>1</sup>*Jet Propulsion Laboratory, California Institute of Technology, Pasadena, California, USA*

<sup>2</sup>*Goddard Space Flight Center, Greenbelt, Maryland, USA*

**Abstract** – The second-degree zonal tide raising potential is symmetric about the polar axis and hence can excite the Earth's polar motion only through its action upon non-axisymmetric features of the Earth such as the oceans. In the long-period tidal band, spectral peaks occur at the fortnightly tidal frequencies in power spectra of polar motion excitation observations from which atmospheric effects have been removed. Different observed polar motion excitation series are studied, and different methods of removing atmospheric effects from the polar motion excitation observations are explored in order to assess the robustness of the resulting empirical models for the observed effect of long-period ocean tides on polar motion excitation. At fortnightly frequencies, the various observed empirical models are found to agree with each other to within about  $1\sigma$ . However, improved observations of the effect of fortnightly ocean tides on polar motion excitation are required since the observed effects at the Mf and Mf' tidal frequencies are not consistent with the expectation that the oceans should have the same relative response to the tidal potential at these two nearby tidal frequencies. The observations are then compared with predictions of three ocean tide models: two purely hydrodynamic models and one estimated from Topex/Poseidon altimetric sea surface height measurements. At the fortnightly tidal frequencies, the three ocean tide models predict polar motion excitation amplitudes that differ from each other and from the observations by factors as large as 2, and phases that differ by more than  $100^\circ$ . This illustrates the need for improved models for the effect of long-period ocean tides on polar motion excitation. © 1998 Elsevier Science Ltd. All rights reserved

### 1. INTRODUCTION

Since the Earth's rotation axis is not aligned with its symmetry axis, the Earth wobbles as it rotates. This wobbling motion of the solid Earth, also known as polar motion, is forced by (1) exchange of nonaxial angular momentum between the solid Earth and the Earth's fluid components, and by (2) deformation of the solid Earth (for reviews see, e.g., MUNK and MACDONALD, 1960; LAMBECK, 1980, 1988; MORITZ and MUELLER, 1988; EUBANKS, 1993). Tidally induced deformations of the solid Earth arising from the second degree zonal tide potential cause changes in the Earth's rate of rotation (e.g., YODER *et al.*, 1981); but since this potential is symmetric about the polar axis, tidal deformations of the axisymmetric solid Earth cannot cause polar motion. However, due to the non-axisymmetric shape of the coastlines, the tide-raising potential acting on the oceans can generate polar motion via exchange of nonaxial ocean tidal angular momentum with the solid Earth.

The observed polar motion at nearly diurnal prograde and nearly semidiurnal prograde and retrograde frequencies has been shown to be dominantly caused by ocean tidal forcing (SOVERS *et al.*, 1993; HERRING and DONG, 1994; WATKINS and EANES, 1994; CHAO *et al.*, 1996; GIPSON,

1996). CHAO (1994) and GROSS *et al.* (1996) have recently presented evidence that ocean tides in the long-period tidal band also measurably cause polar motion, particularly at fortnightly frequencies. This report extends the earlier results of CHAO (1994) and GROSS *et al.* (1996) by utilizing improved polar motion and atmospheric angular momentum data sets that have recently become available, by exploring different means of removing atmospheric effects from the polar motion observations prior to extracting the ocean tidal effects, and by comparing the observed ocean tidal effect on polar motion with that predicted not only by purely hydrodynamic ocean tide models, but also by an ocean tide model estimated from Topex/Poseidon altimetric sea surface height measurements (DESAI and WAHR, 1995; DESAI, 1996). The methodology employed in this report is only briefly described here since it closely follows that of GROSS *et al.* (1996) to which interested readers are referred for greater detail.

## 2. OBSERVATIONS

### 2.1. Polar motion excitation data

The complex-valued polar motion excitation function, or chi-function, is the polar motion forcing function that, at frequencies far from the Free Core Nutation resonance (a resonance in polar motion of nearly diurnal retrograde frequency), is related to polar motion through the expression (e.g., GROSS, 1992):

$$\mathbf{p}(t) + \frac{i}{\sigma_{cw}} \frac{d\mathbf{p}(t)}{dt} = \chi(t) \quad (1)$$

where  $i \equiv \sqrt{-1}$ ,  $\mathbf{p}(t) \equiv p_1(t) - i p_2(t)$  where  $p_1(t)$  and  $p_2(t)$  are the  $x$ - and  $y$ -components, respectively, of polar motion,  $\chi(t) \equiv \chi_1(t) + i \chi_2(t)$  where  $\chi_1(t)$  and  $\chi_2(t)$  are the  $x$ - and  $y$ -components, respectively, of the polar motion excitation function, and  $\sigma_{cw}$  is the complex-valued frequency of the Chandler wobble. Note that by convention the positive  $p_2$  direction is defined to be along the meridian at  $90^\circ$  W longitude, whereas the positive  $\chi_2$  direction is taken to be along the meridian at  $90^\circ$  E longitude, thus explaining the minus sign in the above definition of  $\mathbf{p}(t)$ . Equation (1) is an expression of forced simple harmonic motion in the complex plane with the location of the pole in the complex plane being specified by  $\mathbf{p}(t)$  and with the right-hand-side being the forcing function. The forcing function, also known as the excitation or chi-function, is a function of the processes causing the pole position to change which in the present study is the exchange of the angular momentum of the long-period ocean tides with that of the solid Earth.

Comparisons between modeled and observed polar motion can be done either in the wobble domain or in the excitation domain although it is generally preferable to use the excitation domain (e.g., CHAO, 1985). Here, the comparison will be done in the excitation domain; thus, the excitation function  $\chi(t)$  must be recovered from the observed pole position  $\mathbf{p}(t)$ . The polar motion excitation data used here is that associated with SPACE95 (GROSS, 1996; GROSS *et al.*, 1997). SPACE95 is a Kalman filter-based combination of independent Earth orientation measurements taken by the space-geodetic techniques of lunar laser ranging, satellite laser ranging, very long baseline interferometry, and the global positioning system. The Kalman filter used in generating SPACE95 contains a model of the polar motion process (MORABITO *et al.*,

1988) and, besides producing daily estimates of polar motion and universal time, also produces daily estimates of the polar motion excitation functions used in this study.

A multi-taper power spectrum of the SPACE95 polar motion excitation function spanning 1979–1995 is shown in Fig. 1(a). Multi-taper power spectra, by design, provide minimum leakage and robust spectral estimates (THOMSON, 1982). Here, seven orthogonal tapers with a time-bandwidth product of  $4\pi$  are applied. Positive frequencies in Fig. 1 correspond to prograde (counterclockwise) motion of the pole in the complex plane, negative frequencies to retrograde (clockwise) motion. Spectral peaks appear at the prograde and retrograde fortnightly frequencies [ $\pm 26.7$  cycles per year (cpy)], the prograde and retrograde termensual frequencies ( $\pm 40.0$  cpy), but not at the monthly frequencies ( $\pm 13.3$  cpy).

## 2.2. Removal of atmospheric effects

Prior to analyzing the SPACE95 polar motion excitation series for ocean tidal effects, significant sources of nontidal polar motion excitation should be removed, such as those caused by atmospheric wind and pressure fluctuations. All three components of the atmospheric angular momentum (AAM) are routinely computed from products of numerical weather prediction centers and are archived at the International Earth Rotation Service (IERS) Sub-Bureau for Atmospheric Angular Momentum (SALSTEIN *et al.*, 1993). The particular AAM data set chosen for use here is that recently computed by SALSTEIN (1996) from the products of the National Centers for Environmental Prediction (NCEP)/National Center for Atmospheric Research (NCAR) reanalysis system (KALNAY *et al.*, 1996). The NCEP/NCAR reanalysis AAM values used here span January 1, 1979 to December 31, 1995 at 6-hour intervals, have no missing values, and have no discontinuities that are commonly present in other AAM series since the atmospheric general circulation model used in the reanalysis effort was purposely frozen in order to generate homogenous products.

SALSTEIN (1996) has computed the angular momentum associated with atmospheric pressure changes under two different assumptions for the response of the oceans to the imposed atmospheric pressure changes. The oceans are assumed to respond either as (1) an inverted barometer in which case only the mean pressure over the world's oceans is transmitted to the underlying ocean-bottom crust, or (2) a rigid body thereby fully transmitting the imposed atmospheric pressure variations to the ocean-bottom crust. At the periods of interest to this study (a week to a month) the oceans are generally believed to respond as an inverted barometer (e.g., DICKMAN, 1988; PONTE *et al.*, 1991; PONTE, 1992, 1993, 1994) and hence this version of the AAM pressure term was chosen for use here.

The total effect of atmospheric wind and pressure changes was formed by summing the AAM wind (*w*) and pressure terms, with the pressure term being that computed under the inverted barometer (*ib*) approximation. Daily averages of the four-times-per-day AAM values were formed with the daily averaged AAM values then linearly projected to midnight prior to their removal from the observed polar motion excitation series (which is given as daily values at midnight). Figure 1(b) shows the multi-taper power spectrum of the residual series formed upon subtracting the resulting AAM series from the SPACE95 polar motion excitation series. Spectral peaks still appear at the prograde and retrograde fortnightly frequencies, but are no longer evident at the termensual frequencies (compare with Fig. 1(a)).

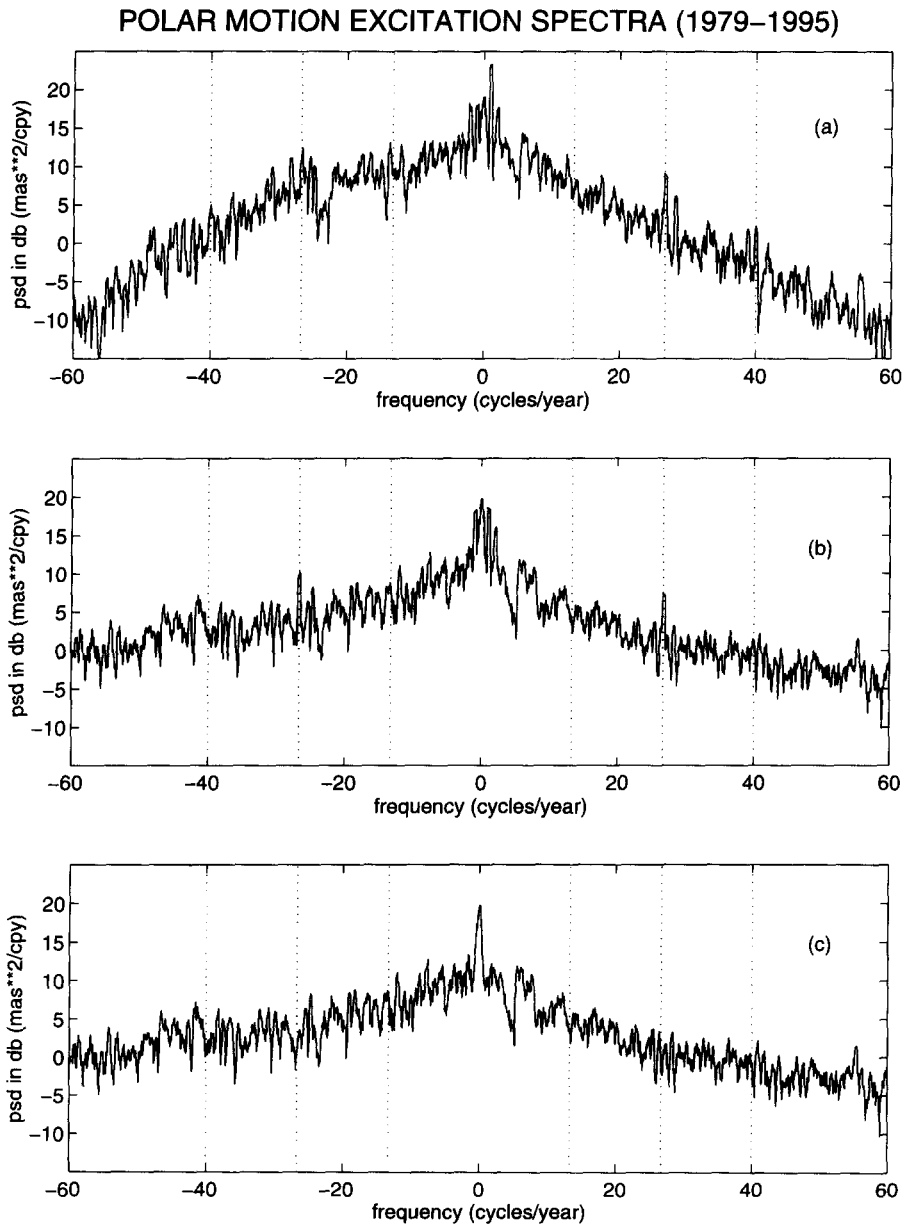


Fig. 1. Multi-taper power spectral density (psd) estimates in decibels (db) computed from time series of polar motion excitation functions  $\chi(t)$  spanning 1979–1995 of: (a) the SPACE95 polar motion excitation function derived from space-geodetic Earth rotation measurements, (b) the residual polar motion excitation function formed by subtracting atmospheric effects from the SPACE95 excitation series, and (c) the result of removing the recovered tidal terms from the SPACE95-AAM residual series. The vertical dotted lines indicate frequencies in the prograde and retrograde termensual tidal bands (at  $\pm 40.0$  cpy), fortnightly tidal bands (at  $\pm 26.7$  cpy), and monthly tidal bands (at  $\pm 13.3$  cpy). The retrograde (clockwise) component of polar motion excitation is represented by negative frequencies, the prograde (counterclockwise) component by positive frequencies.

### 2.3. Recovery of ocean tidal terms

Besides fitting for periodic terms at the tidal frequencies listed in Table 1, the least-squares fit to the SPACE95-AAM residual polar motion excitation series also included terms for the mean and trend of the series. The entries labeled "SP95 - [w + ib]" in Table 2 give the results and  $1\sigma$  formal errors of the fit for the tidal terms at the termensual, fortnightly, and monthly frequencies in terms of the amplitude  $A$  and phase  $\alpha$  of the prograde and retrograde components of the polar motion excitation function defined by:

$$\chi(t) = A_p e^{i\alpha_p} e^{i\phi(t)} + A_r e^{i\alpha_r} e^{-i\phi(t)} \quad (2)$$

where the subscript  $p$  denotes prograde, the subscript  $r$  denotes retrograde, and  $\phi(t)$  represents the tidal argument, the expansion of which is given in Table 1 for each tidal frequency considered here. The results of the fit at the semiannual and annual tidal frequencies are not given in Table 2 since they include such unmodeled, nontidal polar motion excitation effects as seasonal changes in the wind-driven circulation of the oceans.

The two fortnightly terms, as are the two termensual terms, are close to each other in frequency, being separated by just the lunar nodal frequency  $\Omega$  (1/18.6 cpy; see Table 1). Generally speaking, a time series spanning at least 18.6 years would be required to resolve two tidal terms separated in frequency by 1/18.6 cpy. However, these terms have been reasonably well-resolved in the fit to the 16-year-long SPACE95-AAM residual polar motion excitation series as evidenced by an examination of the covariance matrix of the fit which shows that the largest correlation, in absolute value, between the solved-for periodic parameters is 0.09. The fact that these tidal terms have been resolved in a series spanning less than 18.6 years is an example of what MUNK and HASSELMANN (1964) call "super-resolution".

Figure 1(c) shows the multi-taper power spectrum of the post-fit residual series. As expected, there are no longer any spectral peaks at the fortnightly frequencies. Spectra (not shown) of subsets of the post-fit residual series spanning shorter lengths of time (ranging in length from 1.5 years to 10 years) also do not exhibit peaks at the fortnightly frequencies, indicating that

Table 1. Expansion of the tidal argument

| Tide        | Period (solar days) | Fundamental argument |      |     |     |          |
|-------------|---------------------|----------------------|------|-----|-----|----------|
|             |                     | $l$                  | $l'$ | $F$ | $D$ | $\Omega$ |
| Termensual  |                     |                      |      |     |     |          |
| Mt'         | 9.12                | 1                    | 0    | 2   | 0   | 1        |
| Mt          | 9.13                | 1                    | 0    | 2   | 0   | 2        |
| Fortnightly |                     |                      |      |     |     |          |
| Mf'         | 13.63               | 0                    | 0    | 2   | 0   | 1        |
| Mf          | 13.66               | 0                    | 0    | 2   | 0   | 2        |
| Monthly     |                     |                      |      |     |     |          |
| Mm          | 27.55               | 1                    | 0    | 0   | 0   | 0        |
| Semiannual  |                     |                      |      |     |     |          |
| Ssa         | 182.62              | 0                    | 0    | 2   | -2  | 2        |
| Annual      |                     |                      |      |     |     |          |
| Sa          | 365.26              | 0                    | 1    | 0   | 0   | 0        |

Table 2. Observed and predicted effects of long-period ocean tides on the polar motion excitation function  $\chi(t)$ 

|   | Prograde        |                 | Retrograde      |                 |
|---|-----------------|-----------------|-----------------|-----------------|
|   | Amplitude (mas) | Phase (degrees) | Amplitude (mas) | Phase (degrees) |
| Mt' (9.12-day)                                |                 |                 |                 |                 |
| SP95 - [w + ib]                               | 0.68 ± 0.30     | -6 ± 25         | 0.60 ± 0.30     | 141 ± 28        |
| SP95 - [w + $\gamma$ ib + (1 - $\gamma$ )nib] | 0.55 ± 0.31     | 1 ± 32          | 0.50 ± 0.31     | 123 ± 36        |
| SP94 - [w + ib] <sup>1</sup>                  | 0.54 ± 0.45     | 38 ± 48         | 0.21 ± 0.45     | 79 ± 126        |
| Dickman model <sup>2</sup>                    | 0.13            | 73              | 0.21            | 15              |
| Mt (9.13-day)                                 |                 |                 |                 |                 |
| SP95 - [w + ib]                               | 0.22 ± 0.30     | 19 ± 78         | 0.33 ± 0.30     | - 37 ± 52       |
| SP95 - [w + $\gamma$ ib + (1 - $\gamma$ )nib] | 0.16 ± 0.31     | 19 ± 115        | 0.41 ± 0.31     | - 78 ± 44       |
| SP94 - [w + ib] <sup>1</sup>                  | 0.47 ± 0.45     | - 30 ± 55       | 0.41 ± 0.45     | - 95 ± 63       |
| Dickman model <sup>2</sup>                    | 0.32            | 73              | 0.52            | 15              |
| Mf' (13.63-day)                               |                 |                 |                 |                 |
| SP95 - [w + ib]                               | 1.37 ± 0.30     | 30 ± 13         | 1.36 ± 0.30     | 69 ± 13         |
| SP95 - [w + $\gamma$ ib + (1 - $\gamma$ )nib] | 1.27 ± 0.31     | 30 ± 14         | 1.50 ± 0.31     | 59 ± 12         |
| SP94 - [w + ib] <sup>1</sup>                  | 1.61 ± 0.45     | 56 ± 16         | 2.01 ± 0.45     | 87 ± 13         |
| Dickman model <sup>2</sup>                    | 0.52            | 100             | 0.71            | 8               |
| Brosche/Seiler/Gross model <sup>3</sup>       | 0.72            | 55              | 0.59            | 72              |
| Mf (13.66-day)                                |                 |                 |                 |                 |
| SP95 - [w + ib]                               | 1.69 ± 0.30     | 116 ± 10        | 2.58 ± 0.30     | 31 ± 7          |
| SP95 - [w + $\gamma$ ib + (1 - $\gamma$ )nib] | 1.60 ± 0.31     | 116 ± 11        | 2.59 ± 0.31     | 36 ± 7          |
| SP94 - [w + ib] <sup>1</sup>                  | 0.86 ± 0.45     | 93 ± 30         | 2.73 ± 0.45     | 14 ± 10         |
| Dickman model <sup>2</sup>                    | 1.26            | 100             | 1.72            | 8               |
| Brosche/Seiler/Gross model <sup>3</sup>       | 1.72            | 55              | 1.44            | 72              |
| Desai & Wahr model (10-110) <sup>4</sup>      | 3.41            | 158             | 1.73            | - 4             |
| Desai & Wahr model (10-130)                   | 3.07            | 170             | 2.45            | 4               |
| Mm (27.55-day)                                |                 |                 |                 |                 |
| SP95 - [w + ib]                               | 0.65 ± 0.30     | 95 ± 26         | 0.98 ± 0.30     | -55 ± 17        |
| SP95 - [w + $\gamma$ ib + (1 - $\gamma$ )nib] | 0.61 ± 0.31     | 140 ± 30        | 0.88 ± 0.31     | - 53 ± 20       |
| SP94 - [w + ib] <sup>1</sup>                  | 0.75 ± 0.45     | 49 ± 35         | 0.82 ± 0.45     | - 59 ± 32       |
| Dickman model <sup>2</sup>                    | 0.47            | 136             | 0.28            | - 7             |
| Brosche/Seiler/Gross model <sup>3</sup>       | 0.78            | 74              | 0.92            | 28              |
| Desai & Wahr model (10-110) <sup>4</sup>      | 1.15            | - 50            | 0.90            | 153             |
| Desai & Wahr model (10-130)                   | 1.22            | - 34            | 0.43            | 24              |

<sup>1</sup>As reported by GROSS *et al.* (1996).<sup>2</sup>From the ocean tidal effect on polar motion reported by DICKMAN (1993). See GROSS *et al.* (1996) for a discussion of these results.<sup>3</sup>From the ocean tidal effect on polar motion reported by GROSS (1993) and computed from the angular momenta of the Brosche ocean tide model as tabulated by SEILER (1991).<sup>4</sup>From the ocean tidal effect on polar motion reported by DESAI (1996).

these signals in the SPACE95-AAM residual series (Fig. 1(b)) are both (1) phase coherent over 1979–1995 and (2) can be represented by the empirical model given in Table 2. The phase coherence of the fortnightly signals over a period of 16 years strongly indicates that they are of tidal origin.

Also shown in Table 2 are two additional empirical models for the effect of long-period ocean tides on polar motion excitation. The first, labeled “SP94 – [w + ib]”, is that determined by GROSS *et al.* (1996) from the SPACE94-AAM residual polar motion excitation series spanning 1976.8–1994. The AAM series used by them consisted of the sum of the wind and inverted barometer pressure terms computed from the products of the operational NCEP analysis system (not the reanalysis system whose products are used here). The second, labeled “SP95 – [w +  $\gamma$ ib + (1 –  $\gamma$ )nib]”, is the result of testing a different method of removing atmospheric effects from the polar motion excitation series. In reality, the oceans respond dynamically to imposed atmospheric pressure variations; the inverted barometer and rigid ocean assumptions are merely two extreme end-members of the spectrum of possible models for the dynamic response of the oceans. Even though the inverted barometer assumption appears to be valid at periods longer than a few days, it is still worthwhile to test this assumption, which is done here by modeling the AAM pressure term as a linear combination of the pressure terms computed under the inverted barometer and rigid ocean (or no inverted barometer, nib) hypotheses, and solving for the value of the linear combination coefficient. The linear combination coefficient  $\gamma$  was determined by a separate least-squares fit to the  $x$ - and  $y$ -components of the SPACE95 polar motion excitation series modeled as:

$$\chi_{pm} = \chi_w + \gamma\chi_{ib} + (1 - \gamma)\chi_{nib} \quad (3)$$

where  $\chi_{pm}$  is either the  $x$ - or  $y$ -component of the SPACE95 polar motion excitation series,  $\chi_w$  is that respective component of the AAM wind term computed from the NCEP/NCAR reanalysis products,  $\chi_{ib}$  is that respective component of the AAM pressure term computed under the inverted barometer assumption, and  $\chi_{nib}$  is that respective component of the AAM pressure term computed under the rigid ocean, or no inverted barometer, assumption. The value obtained for the linear combination coefficient  $\gamma$  was 0.7603 for the  $x$ -component and 0.4947 for the  $y$ -component. The empirical model for the effect of long-period ocean tides on polar motion excitation obtained by removing this linear combination of the atmospheric wind and pressure terms from the SPACE95 polar motion excitation series prior to solving for the tidal terms is reported in Table 2 under the entries labeled “SP95 – [w +  $\gamma$ ib + (1 –  $\gamma$ )nib]”.

As can be seen from Table 2, the various estimates for the observed effect of long-period ocean tides on polar motion excitation agree with each other to within about 1–2 $\sigma$ , with the various estimates at the fortnightly frequencies agreeing with each other to within about 1 $\sigma$ . The preferred empirical model, however, is that resulting from removing the sum of the AAM wind and inverted barometer pressure terms from the SPACE95 polar motion excitation series since these results generally have the smallest formal uncertainties. Furthermore, since the formal uncertainties are computed from the root-mean-square (rms) scatter of the post-fit residual series, the results with the smallest formal uncertainties will be those determined from the series with the smallest rms scatter, that is, from the series that has had atmospheric effects removed most completely (assuming here that the various mechanisms exciting polar motion are uncorrelated with each other). Thus, at the frequencies of interest here, atmospheric effects are better modeled by taking the sum of the wind and inverted barometer pressure terms than they are by taking the sum of the wind and the best-fitting linear combination of inverted barometer and no inverted

barometer pressure terms. This is confirmed by an examination (not shown) of power spectra of the respective SPACE95-AAM residual series which indicates generally smaller power in that series from which the sum of the wind and inverted barometer pressure terms has been removed.

### 3. MODEL PREDICTIONS

The predictions of three different ocean tide models for the effect of long-period ocean tides on polar motion excitation are also given in Table 2. The first two predictions are from purely hydrodynamic ocean tide models: that of DICKMAN (1993), and that of Brosche as analyzed by SEILER (1991) for ocean tidal angular momenta and subsequently by GROSS (1993), BROSCHE and WÜNSCH (1994), and SEILER and WÜNSCH (1995) for the ocean tidal effect on polar motion (the entries in Table 2 for the predictions of these two ocean tide models have been reproduced here from those given by GROSS *et al.* (1996) where greater discussion of these model predictions can be found).

The third ocean tide model whose polar motion excitation predictions are listed in Table 2 is that of Desai and Wahr (DESAI and WAHR, 1995; DESAI, 1996) whose model has been estimated from Topex/Poseidon altimetric sea surface height measurements taken between latitudes 66°S to 66°N, and then extended to the poles using the hydrodynamic ocean tide model of SCHWIDERSKI (1980a, b). The Desai and Wahr model estimates tidal solutions from the Topex/Poseidon altimetric measurements in geographic bins of size  $360/127 \approx 3$  degrees in longitude and 1 degree in latitude, which are then smoothed and interpolated to a 1 degree by 1 degree grid. The model estimates a smooth response function in each of the diurnal and semidiurnal tidal bands, a constant response function in each of the monthly, fortnightly, and termensual (9-day) tidal bands, and the harmonic response at each of the semiannual and annual frequencies. The smooth response functions implicitly assume a smooth relative response between tidal components whose frequencies lie within the bandwidths of each response function. The bandwidth of the response function in the monthly tidal band includes all tidal components with frequencies from 0.0285498645 cycles per day to 0.0445052444 cycles per day, and similarly the bandwidth of the response function in the fortnightly tidal band includes all tidal components with frequencies from 0.0628694738 cycles per day to 0.0789722089 cycles per day. Therefore, the Desai and Wahr model implicitly separates the ocean tide response of the  $M_f$  and  $M_f'$  tidal components by assuming a constant relative response between these two components.

Two different results from the Desai and Wahr model are listed in Table 2 corresponding to two different time spans of Topex data used in the model estimation procedure: Topex repeat cycles 10–110 (approximately 1000 days), and Topex repeat cycles 10–130 (approximately 1200 days). If the predictions from the Desai and Wahr model have converged, then the entries in Table 2 for repeat cycles 10–130 should be nearly the same as those for repeat cycles 10–110. The predictions for these two cases at the prograde  $M_f$  and  $M_m$  frequencies agree reasonably well with each other, with phases differing by only 12° and 16°, respectively, and amplitudes differing by only 10% and 6%, respectively. However, the disagreements in the predictions at the retrograde  $M_f$  and  $M_m$  frequencies are much larger, with phases differing by 8° and 129°, respectively, and amplitudes differing by 29% and 52%, respectively.

The convergence properties of the predictions of the Desai and Wahr model are illustrated in the phasor diagrams of Fig. 2 which show the amplitude and phase of the predicted effect of the  $M_m$  and  $M_f$  ocean tides on polar motion as a function of the amount of Topex data that

### Polar Motion Observations and Tide Model Predictions

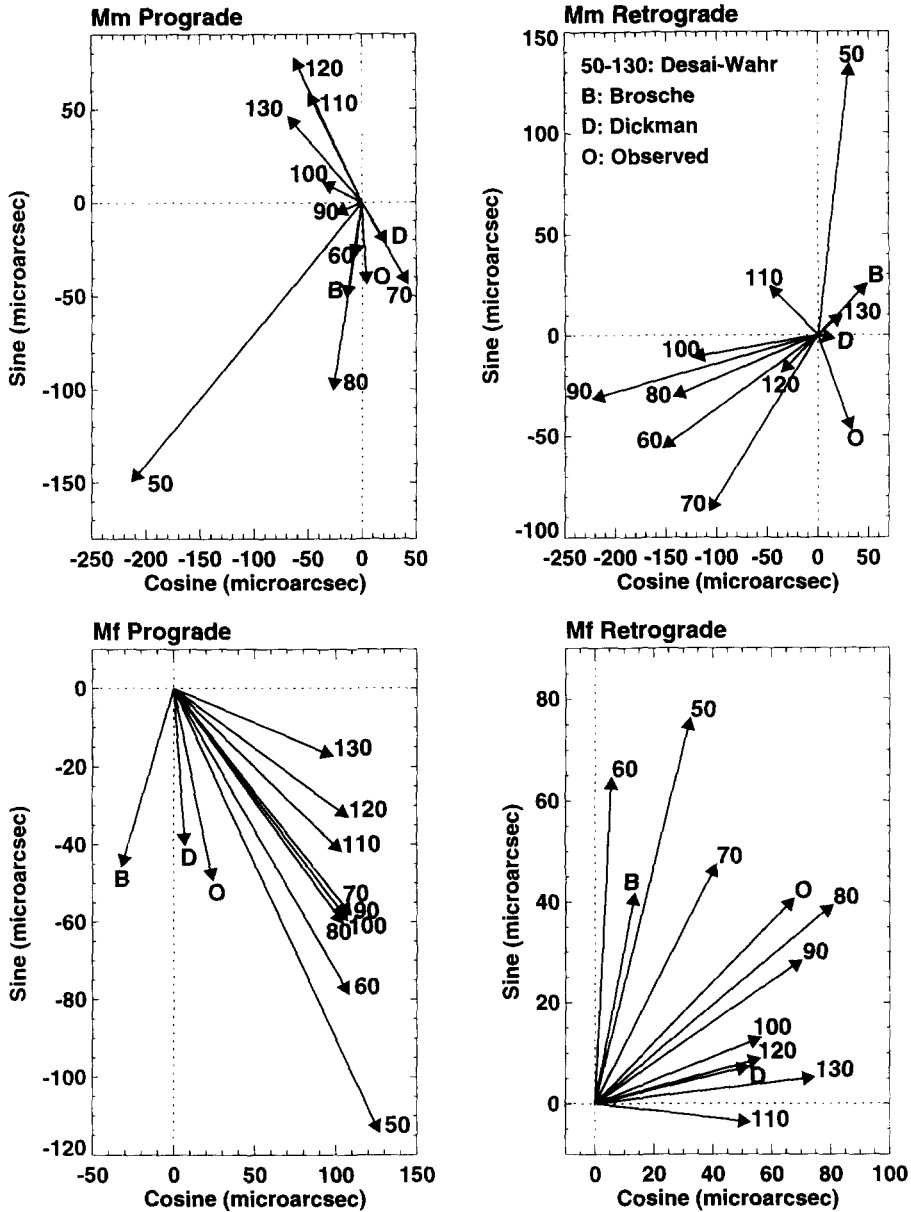


Fig. 2. Phasor diagrams of the amplitude and phase of the effect on polar motion of the Mf and Mm ocean tides predicted by the Desai and Wahr ocean tide model as a function of the duration of Topex/Poseidon data included in the estimation of the model (DESAI, 1996). Arrows labeled "50" are predictions based upon data from Topex/Poseidon repeat cycles 10–50, "60" are based upon repeat cycles 10–60, etc. The arrows labeled "B" are the predictions of the Brosche model as tabulated by GROSS (1993); the arrows labeled "D" are the predictions of DICKMAN (1993); and the arrows labeled "O" are the observed "SP95 – [w + ib]" results of this study (see Table 2). Note that the results illustrated here are for the effect of the Mf and Mm ocean tides on polar motion  $p(t)$ , whereas the results tabulated in Table 2 are for the effect on polar motion excitation  $\chi(t)$ .

has been used in estimating the model. The effect on polar motion  $\mathbf{p}(t)$  was recovered from the effect on polar motion excitation  $\chi(t)$  by solving Eq. (1) with the excitation function given by Eq. (2). The numerical labels in Fig. 2 indicate the amount of Topex data that has been used in estimating the Desai and Wahr model. For example, the arrows labeled "50" have used measurements from Topex cycles 10–50, those labeled "60" have used measurements from cycles 10–60, etc. Also indicated in Fig. 2 are the predictions (labeled "B") of the Brosche tide model, the predictions (labeled "D") of the Dickman tide model, and the observed "SP95 – [w + ib]" results (labeled "O") of this study. As can be seen, the effects of the Mf and Mm ocean tides on polar motion as predicted by the Desai and Wahr model are still changing as additional Topex measurements are incorporated into the model, indicating that the predictions of this model have not yet converged, neither at the prograde nor the retrograde frequencies. In the most extreme case illustrated, the phase of the predicted Mm retrograde tidal effect changes by nearly  $180^\circ$  as sea surface height measurements from 10 additional Topex cycles (120–130) are used in estimating the model.

The fact that the predictions of the Desai and Wahr model have not yet converged may possibly be caused by a combination of the small amplitudes and long periods of the long-period ocean tides with respect to the accuracy and sampling interval of the Topex/Poseidon measurements. An error analysis by DESAI *et al.* (1997), which included tide gauge comparisons of the Desai and Wahr Mm and Mf ocean tide models, suggests that incorporating Topex/Poseidon measurements of longer duration should noticeably improve these models.

#### 4. DISCUSSION

In Fig. 1(b) spectral peaks are clearly evident at the fortnightly tidal frequencies having corresponding amplitude signal-to-noise ratios of about 5 at the prograde Mf tidal frequency, and about 8 at the retrograde Mf tidal frequency (see Table 2 entries labeled "SP95 – [w + ib]"). However, no spectral peaks are evident in Fig. 1(b) at the termensual or monthly tidal frequencies although the least-squares fit at these frequencies had an amplitude signal-to-noise ratio of about 2. This indicates that the formal uncertainties resulting from the least-squares fit are too small and inflating them by a factor of about 2, or to a level of about  $\pm 0.60$  mas, may provide a more realistic estimate of the uncertainty of the observed amplitudes.

The different empirical models for the effect of ocean tides on polar motion excitation, based upon different observed polar motion excitation series and different methods of removing atmospheric effects, agree with each other at the fortnightly frequencies to within about  $1\sigma$ . However, as can be seen from Table 2, the predictions at the fortnightly frequencies of the different ocean tide models differ from each other and from the observations by up to a factor of 2 in amplitude, and more than  $100^\circ$  in phase. This illustrates the need for better models of the effect of long-period ocean tides on polar motion excitation. The Desai and Wahr ocean tide model may yield improved results by using Topex measurements of longer duration in the model estimation procedure (DESAI *et al.*, 1997). Increasing the bin size used to estimate the tidal solution, or even taking zonal averages as done by CARTWRIGHT and RAY (1990) and RAY and CARTWRIGHT (1994) in their estimation of the Mf and Mm tides from Geosat measurements, may help to stabilize the Desai and Wahr tide solution. Also, the path to convergence may be shortened by accounting for the effects of wind-driven sea surface height changes on the Topex/Poseidon measurements prior to being used to estimate the ocean tide model. This can be accomplished by using the sea surface height products of realistic wind-driven general ocean circulation models

such as that of SEMTNER and CHERVIN (1992). Alternatively, other approaches to determining long-period ocean tide models from Topex/Poseidon measurements may prove useful, such as the data assimilation approach taken by EGBERT *et al.* (1994) in determining their diurnal and semidiurnal ocean tide models. Furthermore, since the Topex/Poseidon measurements are restricted to latitudes between 66°S to 66°N, improved models will also be needed in those polar latitudes not sampled by Topex/Poseidon measurements.

In addition, better observations of the effect of the fortnightly ocean tides on polar motion excitation are needed. In principle, the oceans should have the same relative response to the tidal potential at the Mf and Mf' tidal frequencies since these frequencies are so close to each other, differing by only 1/18.6 cpy. This implies that the phase of the effect of the Mf ocean tide on polar motion excitation should be the same as that of the effect of the Mf' ocean tide, and that the ratio of their amplitudes should be the same as the ratio of the amplitudes of the tidal potential at these frequencies. However, from the entries in Table 2 for the preferred empirical model (labeled "SP95 - [w + ib]") it is seen that this is not the case. The Mf-Mf' difference of the prograde and retrograde phases are seen to be 86° and -38°, respectively, and the prograde and retrograde Mf/Mf' amplitude ratios, which should each be 2.4 (e.g., CARTWRIGHT and EDDEN, 1973, Table 1(a)), are 1.2 and 1.9, respectively. Improved observations of the effect of the fortnightly ocean tides on polar motion excitation will be obtained as additional high-quality, space-geodetic measurements are made. Also, during the least-squares fit to the residual polar motion excitation series, constraints could be placed on the solution forcing the recovered Mf and Mf' tidal terms to have the same phase and the expected amplitude ratio of 2.4.

Besides the direct ocean tidal effect on polar motion excitation discussed in this paper, the luni-solar tide raising potential can cause, in principle, other tidally induced changes in polar motion. For instance, again due to the non-axisymmetric shape of the coastlines, tidally induced changes in the Earth's spin rate will cause the off-diagonal elements of the oceans inertia tensor to change, thereby causing an additional ocean tidally induced change in polar motion. DAHLEN (1976, eq. 146) estimates this consequence of spin-wobble coupling to cause polar motion  $\mathbf{p}(t)$  having an amplitude of 2.8 micro-arcsecond ( $\mu\text{as}$ ) per milli-second (ms) change in the length-of-day (lod). For the  $M_2$  tide, Model C of CHAO *et al.* (1995, Table 1) predicts a change in UT1 of amplitude 17.7 micro-second ( $\mu\text{s}$ ), corresponding to an lod change of amplitude 0.214 ms, and hence an induced polar motion  $\mathbf{p}(t)$  of amplitude 0.61  $\mu\text{as}$ . Of greater importance, the luni-solar torque acting on the triaxiality of the Earth (that is, on the difference  $B - A$  of the two equatorial principal moments of inertia) will excite polar motion at nearly diurnal prograde frequencies, with the largest polar motion  $\mathbf{p}(t)$  amplitude predicted to be 7.5  $\mu\text{as}$  at the  $K_1$  tidal frequency (CHAO *et al.*, 1991). Furthermore, since the luni-solar tide raising potential acting upon any non-axisymmetric feature of the Earth can be expected, in principle, to cause tidally induced changes in polar motion, its action on the heterogeneous distribution of mantle material should also excite polar motion. Estimation of the amplitude of such excitation awaits further investigation.

## 5. ACKNOWLEDGEMENTS

We thank R. Ray and two anonymous referees for their helpful comments on the manuscript. The work described here was partially performed at the Jet Propulsion Laboratory, California Institute of Technology, under contract with the National Aeronautics and Space Administration. R. Gross and B. Chao were supported by the Geodynamics and Geopotential Fields program at NASA's

Office of Mission to Planet Earth. S. Desai was supported by the Topex project at the Jet Propulsion Laboratory under contract 958126.

## 6. REFERENCES

- BROSCHÉ P. and WÜNSCH J. (1994) On the "rotational angular momentum" of the oceans and the corresponding polar motion. *Astronomische Nachrichten* **315**, 181–188.
- CARTWRIGHT D.E. and EDDEN A.C. (1973) Corrected tables of tidal harmonics. *Geophysical Journal of the Royal Astronomical Society* **33**, 253–264.
- CARTWRIGHT D.E. and RAY R.D. (1990) Observations of the Mf ocean tide from Geosat altimetry. *Geophysical Research Letters* **17**, 619–622.
- CHAO B.F. (1985) On the excitation of the Earth's polar motion. *Geophysical Research Letters* **12**, 526–529.
- CHAO B.F. (1994) Zonal tidal signals in the Earth's polar motion (abstract). *Eos Transactions of the American Geophysical Union*, **75**(44), Fall Meeting Suppl., 158.
- CHAO B.F., DONG D.N., LIU H.S. and HERRING T.A. (1991) Libration in the Earth's rotation. *Geophysical Research Letters* **18**, 2007–2010.
- CHAO B.F., RAY R.D. and EGBERT G.D. (1995) Diurnal/semidiurnal oceanic tidal angular momentum: Topex/Poseidon models in comparison with Earth's rotation rate. *Geophysical Research Letters* **22**, 1993–1996.
- CHAO B.F., RAY R.D., GIPSON J.M., EGBERT G.D. and MA C. (1996) Diurnal/semidiurnal polar motion excited by oceanic tidal angular momentum. *Journal of Geophysical Research* **101**, 20151–20163.
- DAHLEN F.A. (1976) The passive influence of the oceans upon the rotation of the Earth. *Geophysical Journal of the Royal Astronomical Society* **46**, 363–406.
- DESAI S.D. (1996) Ocean tides from TOPEX/POSEIDON altimetry with some geophysical applications. Ph.D. thesis, University of Colorado, 254 pp.
- DESAI S.D. and WAHR J.M. (1995) Empirical ocean tide models estimated from TOPEX/POSEIDON altimetry. *Journal of Geophysical Research* **100**, 25205–25228.
- DESAI S.D., WAHR J.M. and CHAO Y. (1997) Error analysis of empirical ocean tide models estimated from TOPEX/POSEIDON altimetry. *Journal of Geophysical Research*, in press.
- DICKMAN S.R. (1988) Theoretical investigation of the oceanic inverted barometer response. *Journal of Geophysical Research* **93**, 14941–14946.
- DICKMAN S.R. (1993) Dynamic ocean-tide effects on Earth's rotation. *Geophysical Journal International* **112**, 448–470.
- EGBERT G.D., BENNETT A.F. and FOREMAN M.G.G. (1994) TOPEX/POSEIDON tides estimated using a global inverse model. *Journal of Geophysical Research* **99**, 24821–24852.
- EUBANKS T.M. (1993) Variations in the orientation of the Earth. In: *Contributions of Space Geodesy to Geodynamics: Earth Dynamics*, D.E. SMITH and D.L. TURCOTTE, editors. *American Geophysical Union Geodynamics Series*, **24**, 1–54.
- GIPSON J.M. (1996) Very long baseline interferometry determination of neglected tidal terms in high-frequency Earth orientation variation. *Journal of Geophysical Research* **101**, 28051–29064.
- GROSS R.S. (1992) Correspondence between theory and observations of polar motion. *Geophysical Journal International* **109**, 162–170.
- GROSS R.S. (1993) The effect of ocean tides on the Earth's rotation as predicted by the results of an ocean tide model. *Geophysical Research Letters* **20**, 293–296.
- GROSS R.S. (1996) A combination of EOP measurements: SPACE95. Summarized in: 1995 IERS Annual Report, Obs. de Paris, pp. II11.
- GROSS R.S., HAMDAN K.H. and BOGGS D.H. (1996) Evidence for excitation of polar motion by fortnightly ocean tides. *Geophysical Research Letters* **23**, 1809–1812.
- GROSS R.S., EUBANKS T.M., STEPPE J.A., FREEDMAN A.P., DICKEY J.O. and RUNGE T.F. (1997) A Kalman filter-based approach to combining independent Earth orientation series. *Journal of Geodesy*, in press.
- HERRING T.A. and DONG D. (1994) Measurement of diurnal and semidiurnal rotational variations and tidal parameters of Earth. *Journal of Geophysical Research* **99**, 18051–18071.

- KALNAY E., KANAMITSU M., KISTLER R., COLLINS W., DEAVEN D., GANDIN L., IREDELL M., SAHA S., WHITE G., WOOLLEN J., ZHU Y., CHELLIAH M., EBISUZAKI W., HIGGINS W., JANOWIAK J., MO K.C., LEETMA A., REYNOLDS R., JENNE R. and JOSEPH D. (1996) The NCEP/NCAR 40-year Reanalysis Project. *Bulletin of the American Meteorological Society* **77**, 437–471.
- LAMBECK K. (1980) *The Earth's Variable Rotation: Geophysical Causes and Consequences*. Cambridge University Press, 449 pp.
- LAMBECK K. (1988) *Geophysical Geodesy: The Slow Deformations of the Earth*. Oxford University Press, 718 pp.
- MORABITO D.D., EUBANKS T.M. and STEPPE J.A. (1988) Kalman filtering of Earth orientation changes. In: *The Earth's Rotation and Reference Frames for Geodesy and Geodynamics*, A. K. BABCOCK and G. A. WILKINS, editors. D. Reidel, 257–267.
- MORITZ H. and MUELLER I.I. (1988) *Earth Rotation: Theory and Observation*, Ungar, 617 pp.
- MUNK W.H. and MACDONALD G.J.F. (1960) *The Rotation of the Earth: A Geophysical Discussion*. Cambridge University Press, 323 pp.
- MUNK W.H. and HASSELMANN K. (1964) Super-resolution of tides. In: *Studies on Oceanography*. Hidaka Memorial Volume, Tokyo, 339–344.
- PONTE R.M. (1992) The sea level response of a stratified ocean to barometric pressure forcing. *Journal of Physical Oceanography* **22**, 109–113.
- PONTE R.M. (1993) Variability in a homogenous global ocean forced by barometric pressure. *Dynamics of Atmospheres and Oceans* **18**, 209–234.
- PONTE R.M. (1994) Understanding the relation between wind- and pressure-driven sea level variability. *Journal of Geophysical Research* **99**, 8033–8039.
- PONTE R.M., SALSTEIN D.A. and ROSEN R.D. (1991) Sea level response to pressure forcing in a barotropic numerical model. *Journal of Physical Oceanography* **21**, 1043–1057.
- RAY R.D. and CARTWRIGHT D.E. (1994) Satellite altimeter observations of the Mf and Mm ocean tides, with simultaneous orbit corrections. In: *Gravimetry and Space Techniques Applied to Geodynamics*, B. E. SCHUTZ, A. ANDERSON, C. FROIDEVAUX and M. PARKE, editors. American Geophysical Union Geophysical Monograph Series, **82**, 69–78.
- SALSTEIN D.A. (1996) Sub-bureau for Atmospheric Angular Momentum. In: *1995 IERS Annual Report*. Obs. de Paris, III7–III15.
- SALSTEIN D.A., KANN D.M., MILLER A.J. and ROSEN R.D. (1993) The Sub-bureau for Atmospheric Angular Momentum of the International Earth Rotation Service: A Meteorological Data Center with Geodetic Applications. *Bulletin of the American Meteorological Society* **74**, 67–80.
- SCHWIDERSKI E.W. (1980a) Ocean tides, Part I: Global ocean tidal equations. *Marine Geodesy* **3**, 161–217.
- SCHWIDERSKI E.W. (1980b) Ocean tides, Part II: A hydrodynamical interpolation model. *Marine Geodesy* **3**, 219–255.
- SEILER U. (1991) Periodic changes of the angular momentum budget due to the tides of the world ocean. *Journal of Geophysical Research* **96**, 10287–10300.
- SEILER U. and WÜNSCH J. (1995) A refined model for the influence of ocean tides on UT1 and polar motion. *Astronomische Nachrichten* **316**, 419–423.
- SEMTNER A.J. and CHERVIN R.M. (1992) Ocean general circulation from a global eddy-resolving model. *Journal of Geophysical Research* **97**, 5493–5550.
- SOVERS O.J., JACOBS C.S. and GROSS R.S. (1993) Measuring rapid ocean tidal Earth orientation variations with VLBI. *Journal of Geophysical Research* **98**, 19959–19971.
- THOMSON D.J. (1982) Spectrum estimation and harmonic analysis. *Proceedings of the Institute of Electrical and Electronics Engineers* **70**, 1055–1096.
- WATKINS M.M. and EANES R.J. (1994) Diurnal and semidiurnal variations in Earth orientation determined from LAGEOS laser ranging. *Journal of Geophysical Research* **99**, 18073–18079.
- YODER C.F., WILLIAMS J.G. and PARKE M.E. (1981) Tidal variations of Earth rotation. *Journal of Geophysical Research* **86**, 881–891.